Denis Krnjaca*, Lorena Krames, Matthias Schaufelberger, and Werner Nahm

A Statistical Shape Model Pipeline to Enable the Creation of Synthetic 3D Liver Data

https://doi.org/10.1515/cdbme-2023-1035

Abstract: The application of machine learning approaches in medical technology is gaining more and more attention. Due to the high restrictions for collecting intraoperative patient data, synthetic data is increasingly used to support the training of artificial neural networks. We present a pipeline to create a statistical shape model (SSM) using 28 segmented clinical liver CT scans. Our pipeline consists of four steps: data preprocessing, rigid alignment, template morphing, and statistical modeling. We compared two different template morphing approaches: Laplace-Beltrami-regularized projection (LBRP) and nonrigid iterative closest points translational (N-ICP-T) and evaluated both morphing approaches and their corresponding shape model performance using six metrics. LBRP achieved a smaller mean vertex-to-nearest-neighbor distances (2.486 ± 0.897 mm) than N-ICP-T (5.559 ± 2.413 mm). Generalization and specificity errors for LBRP were consistently lower than those of N-ICP-T. The first principal components of the SSM showed realistic anatomical variations. The performance of the SSM was comparable to a state-of-the-art model.

Keywords: liver, statistical shape model, template morphing, shape analysis, synthetic data

1 Introduction

Machine learning approaches often require a large amount of training data, which can be difficult to obtain, especially in medical image analysis due to difficult acquisition and ethical considerations [1]. Regarding the liver, publicly and off-the-shelf datasets are only sparsely available. In order to overcome this difficulty, the statistical information of the data could be used to synthesize synthetic data. One common approach to create realistic 3D data is using a statistical shape model (SSM) [2].

The work presented by Lamecker et al. [3] is the first 3D SSM of the liver. To solve the 3D correspondence problem, they extended a morphing method algorithm presented in [4]. They used an approach dividing the liver into multiple patches according to the geometry's curvature.

We instead propose an approach relying on landmarks on the liver surface and provide additional metrics such as specificy and vertex-to-nearest-neighbor distance. Automatic preprocessing steps to increase robustness are also included. Our statistical surface model of the liver can be used to generate many three-dimensional organ models. The pipeline consists of re-meshing and hole closing, rigid alignment, template morphing, statistical modeling, and the performance evaluation of two different morphing algorithms. By extending a existing SSM approach to the liver, our pipeline is capable of generating realistic models, providing a possible valuable tool for medical imaging research and applications.

2 Methods

2.1 Dataset and Preprocessing

The dataset consisted of 28 liver 3D CT models, including from the University Hospital in Cologne and the SLIVER07 challenge [5]. Meshlab and its Python-API `pymeshlab` [6] was used to remove isolated parts and duplicated vertices and to smooth the surface of the meshes. We used isotropic explicit remeshing [7] to obtain regular and uniform meshes. The final mean edge lengths are 2 mm for the template and 1 mm for the targets. These steps were performed to reduce the complexity of the dataset and to increase the computation speed and the performance of the morphing step.

2.2 Template Alignment

The alignment of two different shapes required a list of selected feature points as input. Eleven anatomical landmarks were manually placed on the liver surface that corresponded to the same anatomical location on each shape in the training data. The positions of the landmarks on the anterior and posterior side, including their notations, are shown in Fig. 1. The manual placing had to be performed only once during the whole generation process.

To prepare template morphing, the template was initially aligned to each target using the annotated landmarks. Pro-

***Corresponding author: Denis Krnjaca,** Institute of Biomedical Engineering (IBT), Karlsruhe Institute of Technology (KIT), Kaiserstr. 12, 76131 Karlsruhe, Germany, e-mail: publications@ibt.kit.edu
Lorena Krames, Matthias Schaufelberger, Werner Nahm, IBT, KIT, 76131 Karlsruhe, Germany

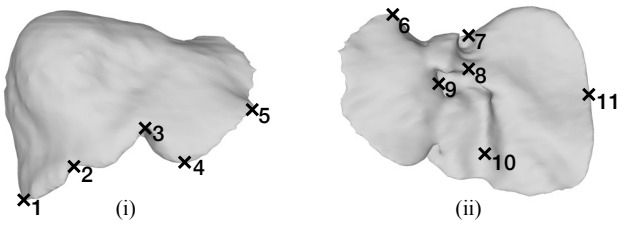

Fig. 1: (i) **Anterior** view of one exemplary liver model with the five placed landmarks: (1) bottom of anterior ridge, (2) gallbladder (fundus), (3) falciform ligament, (4) bottom of left lobe, (5) middle of left lobe. (ii) **Posterior** view with the six placed landmarks: (6) top of left lobe, (7) vena cava (superior), (8) vena cava (inferior), (9) left part of porta hepatis, (10) indentation of gallbladder, (11) middle part of right lobe.

crustes analysis was used to rigidly transform the original template landmarks onto the corresponding target landmarks. By minimizing the Euclidean Procrustes distance between both shapes, the transformation was applied to the whole set of the template points. Note that this process only facilitates template morphing and does neither rescale nor change the target shapes.

2.3 Template Morphing

The two-stage Laplace-Beltrami Regularized Projection (LBRP) was employed to morph the template towards the targets. The core method was presented by [8] and a second morphing step added in [9]. It relies on mutual correspondences between the template and the target. It uses the Laplace-Beltrami operator $\mathbf{L}_0 \in \mathbb{R}^{n_p \times n_p}$ computed on the template as a regularization, controlled by the stiffness parameters λ. The template projection step can be described as follows [8]:

$$\begin{bmatrix} \lambda \mathbf{L}_0 \\ \mathbf{S}_X \end{bmatrix} \mathbf{X} = \begin{bmatrix} \lambda \mathbf{L}_0 \mathbf{X}_0 \\ \mathbf{S}_Y \mathbf{Y} \end{bmatrix}, \tag{1}$$

where $\mathbf{X}_0$ is the initial and $\mathbf{X}$ is the morphed template for which we are solving. The corresponding points *k* for the template and the target are selected by the two Boolean matrices $\mathbf{S}_X \in [0,1]^{k \times n_p}$ and $\mathbf{S}_Y \in [0,1]^{k \times n_t}$, where n_p denotes the number of template, and n_t the number of target vertices. The idea of the method is to perform this template projection twice. First, the projection is employed with a high stiffness parameter $\lambda = 10$ to adapt the template to the target. Afterwards λ is decreased to 1, to enable a more flexible deformation of the template to the target.

To compare this approach with other registration methods, the template morphing was also performed for the nonrigid iterative closest point translational (N-ICP-T) method. The core idea is to solve for a translational transformation of each point and locally regularize transformations of connected points. For detailed explanations, the reader is referred to [10].

2.4 Statistical Modeling

A statistical analysis was performed by computing the sample mean and sample covariance matrix of the training data. To align the morphed templates, a rigid generalized Procrustes analysis (GPA) was employed [2]. GPA iteratively calculates the mean shape of the training data and the deviation of the training data to the calculated mean shape and aligns the training data accordingly. The Euclidean distance was used as the Procrustes distance metric. In this work, scaling was considered as an attribute of shape due to the high variation in size of the liver anatomy. The deformed templates $\mathbf{X}_i \in \mathbb{R}^{p \times 3}$ were reshaped into column vectors $\mathbf{x}_i \in \mathbb{R}^{3p}$. The mean shape $\bar{\mathbf{x}} \in \mathbb{R}^{3p}$ was computed. By subtracting the mean shape from the observations matrix $\mathbf{X}_{\text{Obs}} \in \mathbb{R}^{3p \times 2N}$, the mean-aligned data matrix was obtained. Principal component analysis was used to extract the principal components and reduce the dimensionality of the data.

2.5 Performance Evaluation

Each template morphing approach was evaluated using three metrics: landmark errors, vertex-to-nearest-neighbor distances, and surface normal deviations. Landmark errors provide sparse point-to-point errors on known correspondences. Vertex-to-nearest-neighbor distances evaluate how close the template has been morphed onto the target without taking into account whether the nearest neighbor is morphologically correct. The surface normal deviation evaluates how well point identifiers have been morphed onto morphological similar regions across all deformed templates. For shape model evaluation, the three metrics compactness, generalization and specificity were used. Compactness determines the model's ability to capture most of the variance with few components. Generalization measures the model's ability to fit to unknown observations and specificity the model's ability to create synthetic instances similar to the training data.

3 Results

In Tab. 1 the morphing errors for the two-stage LBRP method and the N-ICP-T method are shown. The LBRP outperformed the N-ICP-T method for the mean vertex-to-nearest-neighbor distance and the mean surface normal deviation. The mean

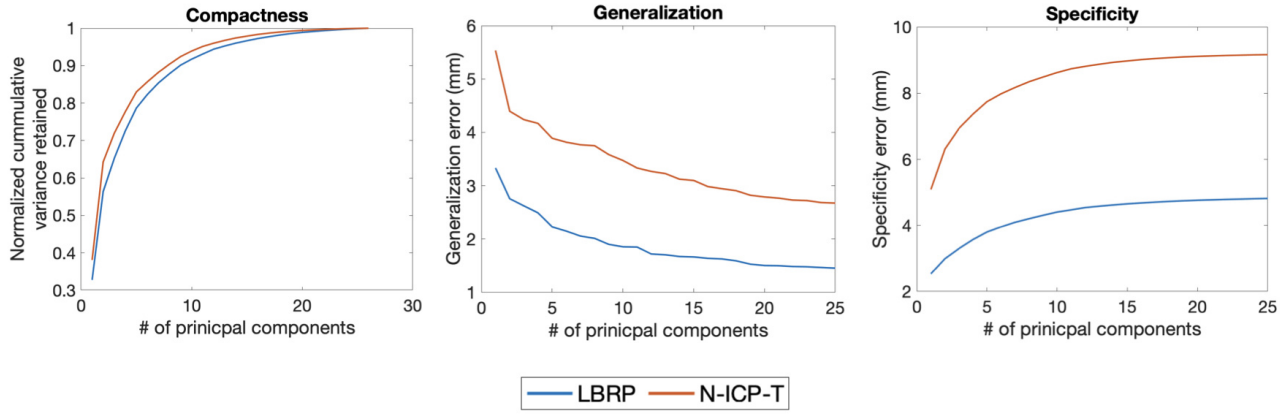

Fig. 2: Shape model metrics for both SSMs as a function of principal components. From left to right: Compactness (higher is better), Generalization and Specificity (lower is better).

Tab. 1: Mean error and standard deviation for both morphing methods.

	LBRP	N-ICP-T
Landmark error (mm)	23.443 ± 5.961	21.968 ± 6.077
Vertex-to-nearest-neigbor-distance (mm)	2.486 ± 0.897	5.559 ± 2.413
Surface normals deviations (°)	22.618 ± 4.613	30.969 ± 9.209

landmark error was lower for the N-ICP-T method. The performance of both final models derived from the morphing algorithms training data are visualized in Fig. 2. The normalized compactness was similar for both SMMs, whereas the generalization and specificity metrics differed for both methods. The LBRP algorithm outperformed the N-ICP-T algorithm. In addition to the performance metrics a qualitative evaluation for the first variations of the final models from the LBRP approach was performed, as shown in Fig. 3. The first mode showed a variation in the height of the liver. Further, a variation in the width of the left and right liver lobes was visible. The second mode showed variations along the anterior ridge and the width of the right liver lobe. In the third mode the most variances were found in the width of the liver lobes. Additionally, a variation in the height of the right liver lobe was visible.

4 Discussion

A pipeline using the two-stage LBRP morphing algorithm was proposed to generate a SSM for the liver. To get a comparison with another registration method, the meshes were also morphed with the N-ICP-T algorithm. The morphing and the shape model evaluation showed that the LBRP approach clearly outperformed the N-ICP-T algorithm. With a smaller mean vertex-to-nearest-neighbor distances of approximately 3 mm and a lower mean surface normal deviation of approximately $8°$, the LBRP considered to be the more promising method. Only for the landmark error, the N-ICP-T method had a slightly lower mean lower error of approximately 1 mm. Landmark errors are typically considered the gold standard, but as the landmarks are placed without any expert knowledge, the metric is deemed less trustworthy for this model. For the compactness of the model both morphing approaches showed similar results. However, the N-ICP-T algorithm appears to be over-fitted in terms of generalization, as it was worse at describing instances outside of the training set. The SSM created with the LBRP algorithm had a better ability to create synthetic instances similar to the training data which is important to improve deep-learning approaches. To evaluate the LBRP algorithm qualitatively, the first mode of the SSMs was analyzed. It showed that the algorithm was able to capture meaningful variations in the liver shape. Moreover, the first modes of the SSM seem to be anatomically correct.

The study of Lamecker et al. [3] used compactness and generalization as performance metrics. The model needed 21 principal components, which corresponds to 48% of the used dataset, to describe 95% of the total variance. The model presented in this work needed 13 principal components which corresponds to 46% of the used dataset, to describe 95% of the total variance. The surface distance errors of the generalization in this work was $1.8\,(\pm 0.5)$ mm, whereas Lamecker et al. obtained an error of $1.9\,(\pm 0.3)$ mm (mean $\pm$ standard deviation σ). However, a direct comparison must be taken with caution due to the use of different datasets and a partly different choice of quantitative metrics.

The most substantial limitation is the small dataset used to train the morphing algorithms. It reduces the performance of

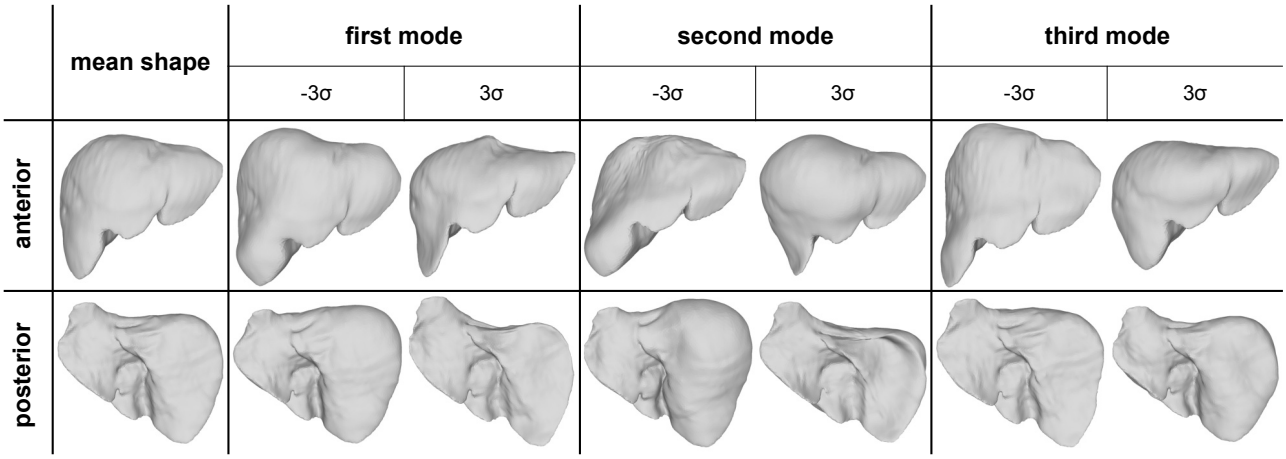

Fig. 3: Mean shape and first three modes of the full model in anterior and posterior view. For the first three models -3σ and 3σ were used.

the SSM by limiting the range of variation seen in the model creation process. With abundant training data, the results in terms of the generalization of the shape model performance would probably improve.

5 Conclusion

We presented a pipeline for the generation of a SSM of the liver which does not rely on manual patch definitions. The SSM captured meaningful variations in the liver shape and showed similar performance to comparable models [3]. The synthesized three-dimensional liver models generated from the SSM can be used to augment preoperative 3D CT data. After validation by clinical experts regarding their anatomical correctness, the model can be used to augment patient cohorts with synthesized samples or to facilitate the development and testing of algorithms for feature and shape analysis.

References

[1] Litjens G, Kooi T, Bejnordi E, Setio A, Ciompi, F, Ghafoorian M, et al. A survey on deep learning in medical image analysis. Medical image analysis; 2017.

[2] Cootes F, Taylor J, Cooper H, Graham J. Training models of shape from sets of examples. In BMVC92: Proceedings of the British Machine Vision Conference. Springer London; 1992.

[3] Lamecker H, Lange T, Seebass M. A statistical shape model for the liver. In Medical Image Computing and Computer-Assisted Intervention—MICCAI 2002; 2022.

[4] Zöckler M, Stalling D, Hege C. Fast and intuitive generation of geometric shape transitions. The Visual Computer; 2000.

[5] Heimann T, Van Ginneken B, Styner A, Arzhaeva Y, Aurich V, Bauer C., et al. Comparison and evaluation of methods for liver segmentation from CT datasets. IEEE transactions on medical imaging; 2009.

[6] Cignoni P, Callieri M, Corsini M, Dellepiane M, Ganovelli F, Ranzuglia G. Meshlab: an open-source mesh processing tool. In Eurographics Italian chapter conference; 2008.

[7] Hugues Hoppe, Tony DeRose, Tom Duchamp, John McDonald, and Werner Stuetzle. Mesh optimization. In Proceedings of the 20th annual conference on Computer graphics and interactive techniques (SIGGRAPH '93). 1993. 10.1145/166117.166119

[8] Dai H, Pears N, Smith W, Duncan C. Statistical modeling of craniofacial shape and texture. International Journal of Computer Vision; 2020.

[9] Schaufelberger M, Kühle R, Wachter A, Weichel F, Hagen N, Ringwald F, Eisenmann U, Hoffmann J, Engel M, Freudlsperger C, Nahm W. A Radiation-Free Classification Pipeline for Craniosynostosis Using Statistical Shape Modeling. Diagnostics. 2022; 12(7):1516. 10.3390/diagnostics12071516

[10] Amberg B, Romdhani S, Vetter T. Optimal step nonrigid ICP algorithms for surface registration. In 2007 IEEE conference on computer vision and pattern recognition; 2007.